CHEMISTRY OF MATERIALS

pubs.acs.org/cm

Article

# $ACd_4Ga_5Te_{12}$ (A = K, Rb, Cs): Tellurides with a Strong Nonlinear Optical Response and Purple Emission

Mengran Sun, Wenhao Xing, Shyong K. Chen, Chunxiao Li, Wenhao Liu, Ming-Hsien Lee,* and Jiyong Yao*

Cite This: *Chem. Mater.* 2023, 35, 7218−7228

Read Online

ACCESS | Metrics & More | Article Recommendations | Supporting Information

**ABSTRACT:** Chalcogenides are promising candidates for exploring mid- and far-infrared nonlinear optical (NLO) materials. Nevertheless, although tellurides possess greater advantages in the above-mentioned spectral regions, the reports on telluride NLO materials are far fewer than those on sulfides and selenides. In this work, a new quaternary NLO-active telluride, $KCd_4Ga_5Te_{12}$, was discovered, and its Rb and Cs analogues were successfully synthesized. They are crystallized in the trigonal *R*3 space group and the structure features a 3D diamond-like framework constructed by vertex-sharing asymmetric $MTe_4$ tetrahedra (centered by disordered Cd and Ga) that are stacked along the *c*-axis. Moreover, a comprehensive study of their IR NLO properties, photoluminescence properties, and structural features was performed. These compounds exhibited large powder second-harmonic generation (SHG) intensities, about 2.1 (2.7, 4.4) times that of $AgGaSe_2$ in the particle size range of 20−50 (125−150) $\mu$m and a wide transmission range (~25 $\mu$m). The SHG-density analysis revealed that the largest component $\chi_{333}^{(2)}$ of $KCd_4Ga_5Te_{12}$ originates from three types of Te in the crystal structure. More importantly, it is rare in literature to demonstrate the consistency of linear and NLO properties calculated using both ultrasoft pseudopotentials and norm-conservation pseudopotentials. Besides, the title compounds also exhibit strong luminescence emissions around 420 and 470 nm at 298 K. This work implies that title compounds are promising candidates in the IR NLO applications.

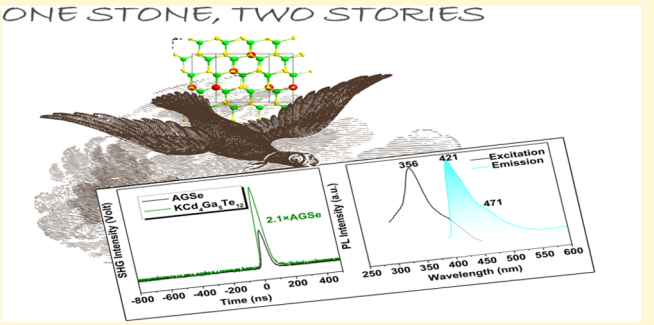


## INTRODUCTION

Stimulated by the increasing demand for the advancement of technology and the progress of modern laser equipment, nonlinear optical (NLO) materials, which can generate the desired coherent light through frequency conversion technology, are widely used in remote sensing, electronic medical, atmospheric detection, laser communication, and so on.[1−11] Generally speaking, NLO materials can be divided into ultraviolet (UV) NLO materials and infrared (IR) NLO materials according to the operation range of the crystals.[12,13] With the rapid increase of mid- and far-IR (MFIR) laser applications in many fields, searching for MFIR NLO crystals has become a research hotspot.[14−20] It is well known that the current commercial IR NLO crystals are $AgGaS_2$ (AGS), $AgGaSe_2$ (AGSe), $ZnGeP_2$ (ZGP), GaSe, $LiGaS_2$, and $LiInSe_2$.[21−26] However, their intrinsic defects limit their higher power applications. Therefore, there is an urgent need to discover new MFIR NLO crystals with high performance.

The non-zero second-order tensor $\chi^{(2)}$ is the prerequisite for the second-harmonic generation (SHG), which is guaranteed by the non-centrosymmetric (NCS) structure.[27,28] Unfortunately, the NCS structure is very rare, as approximately 79% of the inorganic compounds are centrosymmetric (CS) in the Inorganic Crystal Structure Database (ICSD), which is the first challenge in designing the IR NLO candidates.[29] In addition, it is more difficult to investigate some metastable NCS compounds, as we cannot synthesize and evaluate their NLO performances. In recent years, some strategies have been proposed to obtain NCS compounds, including using known NCS structures as templates, element substitution, concentration-driven strategy, structural tolerance factor-guided strategy, etc.[10,30−37] Among them, the chemical substitution of known CS or NCS structures has been proven to be the most effective and simple strategy for designing new excellent IR NLO compounds.[38−41] Selecting an appropriate structural prototype is conducive to the realization of structure−performance regulation. Some examples with favorable NLO properties have been rendered here, encompassing $Pb_4SeBr_6$ (structural prototype: CS $PbBr_2$), $SrCdSiS_4$ (structural

Received: June 15, 2023
Revised: August 14, 2023
Published: August 29, 2023

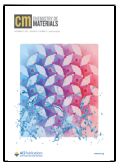

prototype: CS $SrGa_2S_4$), $Sn_7Br_{10}S_2$ (structural prototype: CS $SnBr_2$), $[RbBa_2Cl][Ga_4S_8]$ (structural prototype: CS $RbGaS_2$), $CuZnPS_4$ (structural prototype: NCS $AgGaS_2$), $Ba_3Ge_2O_4Te_3$ (structural prototype: NCS $Ba_2ZnGe_2O_7$), and $Hg_3P_2S_8$ (structural prototype: NCS $Zn_3P_2S_8$).[10,42−47]

Furthermore, the second challenge of designing the IR NLO crystal is how to obtain large nonlinear optical coefficients on the basis of the NCS structure. Chalcogenides have long been the most favorable source of potential IR NLO crystals due to their structural diversity and wide IR transmission range, and a tremendous number of novel candidates have been obtained during the past two decades.[48] In addition, many chalcogenides exhibit large NLO responses, especially those with diamond-like (DL) structural features.[49] Indeed, the fundamental building block $[MQ_4]$ tetrahedron (M = metal cations; Q = S, Se, Te) in the DL structure is always arranged in an aligned manner, which will lead to the superposition of the microscopic second-order susceptibility, resulting in a larger SHG response.[50] For decades, plentiful chalcogenides with a DL structure have been reported, mainly including the I−III−$Q_2$ (I = Li, Ag; III = Al, Ga, In; Q = S, Se, Te) family,[21,22,51] $I_2$−IV−$Q_3$ (I = Ag, Cu; IV = Si, Ge, Sn; Q = S, Se) family,[52−54] $I_3$−V−$Q_4$ (I = Li, Ag, Cu; V = P, As, Sb; Q = S, Se) family,[55] $I_2$−II−IV−$Q_4$ (I = Li, Ag, Cu; II = Zn, Cd, Hg; IV = Si, Ge, Sn; Q = S, Se) family,[56−58] and $I_4$−II−$IV_2$−$Q_7$ (I = Li, Ag; II = Zn, Cd, Hg, Mn; IV = Si, Ge, Sn; Q = S, Se) family.[59,60] However, most of the compounds mentioned above are sulfides and selenides, and tellurides with DL structures are rarely reported. Compared with sulfides and selenides, tellurides generally possess a larger electronic polarization and a wider transmittance range, making them potentially more suitable candidates as MFIR NLO materials.[61]

Based on the above discussion, classical $AgGaTe_2$ was selected as the structural prototype for the exploration of telluride NLO materials with DL structures. Regretfully, although $AgGaTe_2$ possesses a large SHG coefficient ($d_{eff}$ = 77 pm/V) and a wide transmission range (~23 $\mu$m), the light sensitivity of Ag causes a narrow band gap, resulting in a low laser damage threshold, which seriously hinders their further applications.[62] Therefore, Ag atoms are substituted by highly electropositive alkali metals to widen the band gap. Additionally, the transition metal cation $Cd^{2+}$ with a flexible coordination geometry and thermochromism ability is introduced to modulate the properties. Thereby, a new quaternary telluride $KCd_4Ga_5Te_{12}$ with a DL-like structure was successfully discovered. Moreover, although related Rb and Cs compounds were reported with low thermal conductivity in 2016,[63] comprehensive studies of their IR NLO properties and luminescent performance were overlooked. Thus, in this work, three tellurides, $ACd_4Ga_5Te_{12}$ (A = K, Rb, Cs), were synthesized and characterized.

## EXPERIMENTAL SECTION

**Single-Crystal Synthesis.** All starting materials, K (99.99%), Cd (99.99%), Ga (99.99%), RbCl (99.99%), CsCl (99.99%), and Te (99.999%) were directly purchased from Aladdin Co., Ltd. without further purification. The binary raw materials $K_2Te_3$, CdTe, and $Ga_2Te_3$ were synthesized by heating the stoichiometric mixture of the constituent elements in vacuum flame-sealed silica tubes. All manipulations were carried out in an Ar-filled glove box. Single crystals of $KCd_4Ga_5Te_{12}$ were grown from the batches of $K_2Te_3$/CdTe/$Ga_2Te_3$ = 1:3:2. As for the two known $ACd_4Ga_5Te_{12}$ (A = Rb, Cs) compounds, Cd, Ga, and Te were mixed at a molar ratio of 4:5:12 with excess 3 mol ACl as reactive fluxes. These mixtures were loaded into fused-silica tubes and heated to 873 K over 25 h, sustained at 873 K for 10 h, then gradually heated to 1123 K and kept for 50 h, and then cooled to room temperature at a rate of 3 K/h. Finally, several metallic block-shaped crystals $ACd_4Ga_5Te_{12}$ and a small amount of the byproduct $CdGa_2Te_4$ are obtained. The products were washed first with distilled water to remove the excess ACl and chloride byproducts and then dried with ethanol. The single crystals can be stable in air for several months.

**Elemental Analysis.** An FEI Quanta 650FEG scanning electron microscope (SEM) equipped with energy dispersive X-ray (EDX) was used to perform the elemental analysis of $ACd_4Ga_5Te_{12}$ (A = K, Rb, Cs) single crystals. The results indicated the presence of A, Cd, Ga, and Te in the molar ratio of about 1:4:5:12 (Figures S2−S4).

**Single-Crystal X-ray Diffraction.** A $KCd_4Ga_5Te_{12}$ crystal with appropriate morphology was selected for single-crystal X-ray diffraction measurement at 296.15 K on a Rigaku AFC10 diffractometer equipped with a graphite-monochromated Mo K$\alpha$ ($\lambda$ = 0.71073 Å) radiation source. CrysAlispro software was used for data reduction, and the multiscan method was used for absorption correction.[64] Structure solution and refinement of $KCd_4Ga_5Te_{12}$ were carried out with the direct method and full-matrix least squares on $F^2$ with the SHELXL-2014 package.[65] The main crystallographic data and structure refinement details of $KCd_4Ga_5Te_{12}$ are exhibited in Table 1. The atom coordinates and equivalent isotropic displacement parameters are listed in Table S1. The selected bond lengths and angles are listed in Table S3.

**Table 1. Main Crystallographic Data of $KCd_4Ga_5Te_{12}$ and Structure Refinement Parameters[ab]**

| empirical formula | $KCd_4Ga_5Te_{12}$ |
|---|---|
| formula weight | 854.84 |
| crystal system | trigonal |
| space group | *R*3 |
| *T*/K | 296.15 |
| *a*(Å) | 15.4306(6) |
| *b*(Å) | 15.4306(6) |
| *c*(Å) | 10.4666(7) |
| $\alpha$ (°) | 90 |
| $\beta$ (°) | 90 |
| $\gamma$(°) | 120 |
| V(Å$^3$) | 2158.2(2) |
| *Z* | 3 |
| $\rho_{calc}$ (g/cm$^3$) | 5.467 |
| M (mm$^{-1}$) | 19.557 |
| radiation | Mo K$\alpha$ ($\lambda$ = 0.71073) |
| 2$\theta$ range for data | 4.944−60.952 |
| index ranges | $-20 \le h \le 19$, $-21 \le k \le 22$, $-14 \le l \le 14$ |
| reflections collected | 13,797 |
| independent reflections | 2881 [$R_{int}$ = 0.0626, $R_{sigma}$ = 0.0533] |
| GoF on $F^2$ | 1.069 |
| final *R* indexes [$I \ge = 2\sigma$ (*I*)] | $R_1$ = 0.0352, w$R_2$ = 0.0582 |
| final *R* indexes [all data] | $R_1$ = 0.0454, w$R_2$ = 0.0611 |
| Flack parameter | −0.02(4) |

[a] $R(F) = \sum \| |F_o| - |F_c| \| / \sum |F_o|$ for $F_o^2 \ge 2\sigma(F_o^2)$. [b] $R_W(F_o^2) = \{\sum [w(F_o^2 - Fc^2)^2] / \sum wF_o^4\}^{1/2}$ for all data. $w^{-1} = \sigma^2(F_o^2) + (zP)^2$, where $P = (\mathrm{Max}(F_o^2, 0) + 2F_c^2)/3$.

**Powder X-ray Diffraction and Rietveld Refinement.** The phase purity of the powder sample was measured with the use of a Bruker D8 Focus diffractometer equipped with Cu K$\alpha$ ($\lambda$ = 1.5418 Å) radiation. The diffraction pattern was collected from 10 to 70° with the parameters of a scanning step width of 0.02° and a counting time of 0.1 s/step. The experimental powder XRD pattern matches well with the simulated one, indicating the phase purity of the $KCd_4Ga_5Te_{12}$ polycrystalline powder (Figure 1). Furthermore, as


https://doi.org/10.1021/acs.chemmater.3c01493
Chem. Mater. 2023, 35, 7218−7228

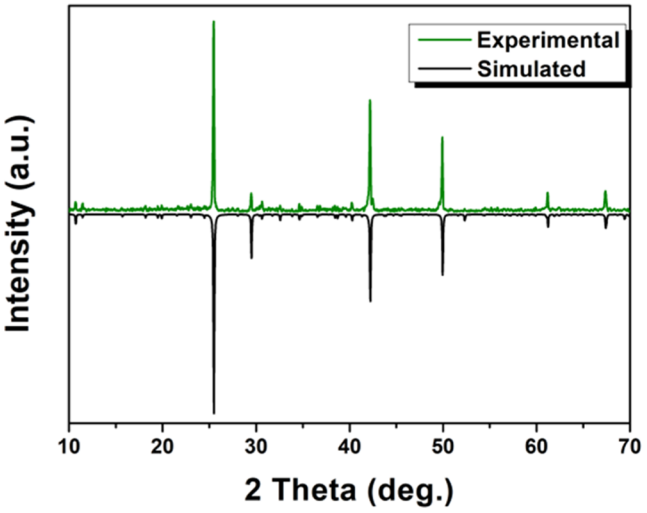


**Figure 1.** Experimental and simulated powder XRD patterns of $KCd_4Ga_5Te_{12}$.

for the two known $ACd_4Ga_5Te_{12}$ (A = Rb, Cs) compounds, the Rietveld refinements of the collected powder X-ray diffraction data were carried out using the GSAS software package with the EXPGUI interface (Figure S1). The results show the phase purity of the synthesized polycrystalline powder. The Rietveld refinement parameters, bond lengths, and angles of $ACd_4Ga_5Te_{12}$ (A = Rb, Cs) obtained by Rietveld refinement are summarized in Tables S4–S6. The unit cell parameters, bond lengths, and angles of the title compounds are in good agreement with the previously reported results, which prove the structural quality of the title compounds.

**Optical Measurements.** A Cary 5000 UV–vis–NIR spectrophotometer with a diffuse-reflectance accessory was applied to obtain the diffuse-reflectance spectra of $KCd_4Ga_5Te_{12}$ and polytetrafluoroethylene (as a reference) in the range of 2500–200 nm. A Lab RAM Aramis spectrometer equipped with a 532 nm laser was used to collect the Raman spectra of $ACd_4Ga_5Te_{12}$ (A = K, Rb, Cs) in the range of 1000 to 100 $cm^{-1}$ at room temperature. An Excalibur 3100 Fourier Transform Infrared Spectrometer collects the IR spectra in the range of 4000–400 $cm^{-1}$. The samples for the IR measurement were prepared by fully grinding the $ACd_4Ga_5Te_{12}$ (A = K, Rb, Cs) powder with the KBr powder (1:100 mass ratio). The solid-state luminescence emission and excitation spectra were recorded on an FLS1000 fluorescence spectrophotometer equipped (Edinburgh Instruments Ltd.) with a continuous Xe-900 xenon lamp. The measurements were implemented in the range of 300–800 nm at room temperature.

**Powder SHG Measurement.** The SHG intensities of $ACd_4Ga_5Te_{12}$ (A = K, Rb, Cs) were estimated by the Kurtz–Perry technique under a 2090 nm illumination generated by a Q-switch Ho:Tm:Cr:YAG laser.[66] The polycrystalline samples of title compounds were sieved into five particle ranges, namely, 20–50, 50–90, 90–125, 125–150, and 150–200 $\mu$m, and then these samples of different particle sizes were loaded into custom holders with a thickness of 1mm. In addition, the single crystals of the traditional material AGSe were fully ground and sieved into the same particle size range as mentioned above for reference.

**Theoretical Calculations.** In this study, CASTEP, a DFT-based plane-wave pseudopotential code, is used for the computational study.[67–69] Model building and input file preparation is done using the Materials Studio graphical user interface. The internal criteria of the latest CASTEP code doing the checking integer value of the total number of electrons has to be set less strictly so that a disorder (mixture atom virtual crystal approximation (VCA)) model is still regarded as a valid insulator. We have made minor modifications to the code to make the calculation work.

VCA is a suitable way to treat disorder/random occupation of sites in a crystalline periodic description, where multiple ions of different species are specified at the same location; a linear combination of each (angular-momentum specific) semilocal pseudopotentials of each participating element is formed and altogether treated as the "effective ion" in later electronic structure calculations. As for the number of the "valence" electrons for the selected atom, it is simply the linear combination of the valence electrons of individual neutral atoms in the same mixing ratio.

A full supercell model avoids the need to handle noninteger numbers of ions, as one usually does when treating defects and impurities in crystalline materials. The nonunity site-occupancy fraction (SOF) is common in experimentally determined CIF (crystal information file). It reflects the disordered nature of the crystal in which the mixture occupancy of some elements is at the same (precise) crystallographic site. This may be due to either sample preparation or simply the nature (geometry/stoichiometry) of the crystal, and no long-range pattern can be further determined by measurement; only the fraction/ratio is certain. However, in the present study, there is an obvious conflict for a compound with the stoichiometry "K $Cd_4$ $Ga_5$ $Te_{12}$" to be fitted inside a crystal system that has a three-fold rotation symmetry. It is, therefore, more elegant to treat the problem under its original space group symmetry; this is the advantage of using VCA.

Norm-conserving optimized pseudopotentials were tested and used in the present study.[70–72] Ga with 13 valence electrons ($3d^{10}4s^24p^1$) must be chosen so that it is compatible with 12 valence electrons of Cd ($4d^{10}5s^2$). VCA mixing between *d*-frozen and *d*-unfrozen atoms will result in an unphysical electronic structure and disaster in computation. The use of an 800 eV kinetic energy cutoff will allow the convergence of total energy to be within 0.1 eV/atom, which is sufficient for the purpose of the present study.

Wavefunction analysis, such as SHG density, usually requires a very fine FFT mesh resolution, which is why norm-conserving pseudopotential was often used. It should not be interpreted as ultrasoft pseudopotentials may not give good results. In the following results section, we will provide an ultrasoft pseudopotential comparison for the same crystal. For achieving good k-point sampling, a separation of 0.017 $Ang^{-1}$ has been chosen for both SCF and optics sum-over-states non-SCF calculations; this results in 60 irreducible *k*-points in the first BZ. Birefringence and SHG coefficients are well converged at this mesh density; we performed calculations with sampling 0.015 and 0.012 $Ang^{-1}$ to confirm this.

The methodology[73–75] the authors used for calculating linear and nonlinear optical properties in the sum-of-states method is similar to previous work, such as $Sr_3Ge_2O_4Te_3$, where detailed references could be found.[36]

## RESULTS AND DISCUSSION

**Crystal Structure.** $KCd_4Ga_5Te_{12}$ was obtained for the first time, and it was crystallized in the *R*3 space group. This crystal is a new member of the enormous $AM_4^{II}M_5^{III}Q_{12}$ (A = K-Cs; $M^{II}$ = $Mn^{2+}$, $Zn^{2+}$, $Cd^{2+}$, $Hg^{2+}$; $M^{III}$ = $Ga^{3+}$, $In^{3+}$; Q = S, Se, Te) compound family.[63,76–79] So far, numerous compounds in this system have been identified, in which $M^{II}$ and $M^{III}$ can accommodate various types of cations, demonstrating the strong inclusiveness of this structural model. The unit cell parameters of $KCd_4Ga_5Te_{12}$ are $a = b = 15.4306(6)$ Å, $c = 10.4666(7)$ Å, and $Z = 3$. In the asymmetric unit, K (Wyckoff sites: 3*a*), Cd/Ga (Wyckoff sites: 9*b*), and Te (Wyckoff sites: 9*b*) occupy one, three, and four crystallography-independent sites, respectively. It is worth noting that all three metal sites in $KCd_4Ga_5Te_{12}$ are disordered by Cd and Ga atoms, with respective occupancies of 0.241–0.601 for Cd and 0.759–0.399 for Ga (Table S1). The oxidation states of K, Cd, Ga, and Te are +1, +2, +3, and −2, respectively, as there is no metal–metal bond or ditelluride bonding in the structure. Moreover, in order to prove the rationality of the structure, the calculated bond valence sums (BVS) and the expected


https://doi.org/10.1021/acs.chemmater.3c01493
Chem. Mater. 2023, 35, 7218–7228

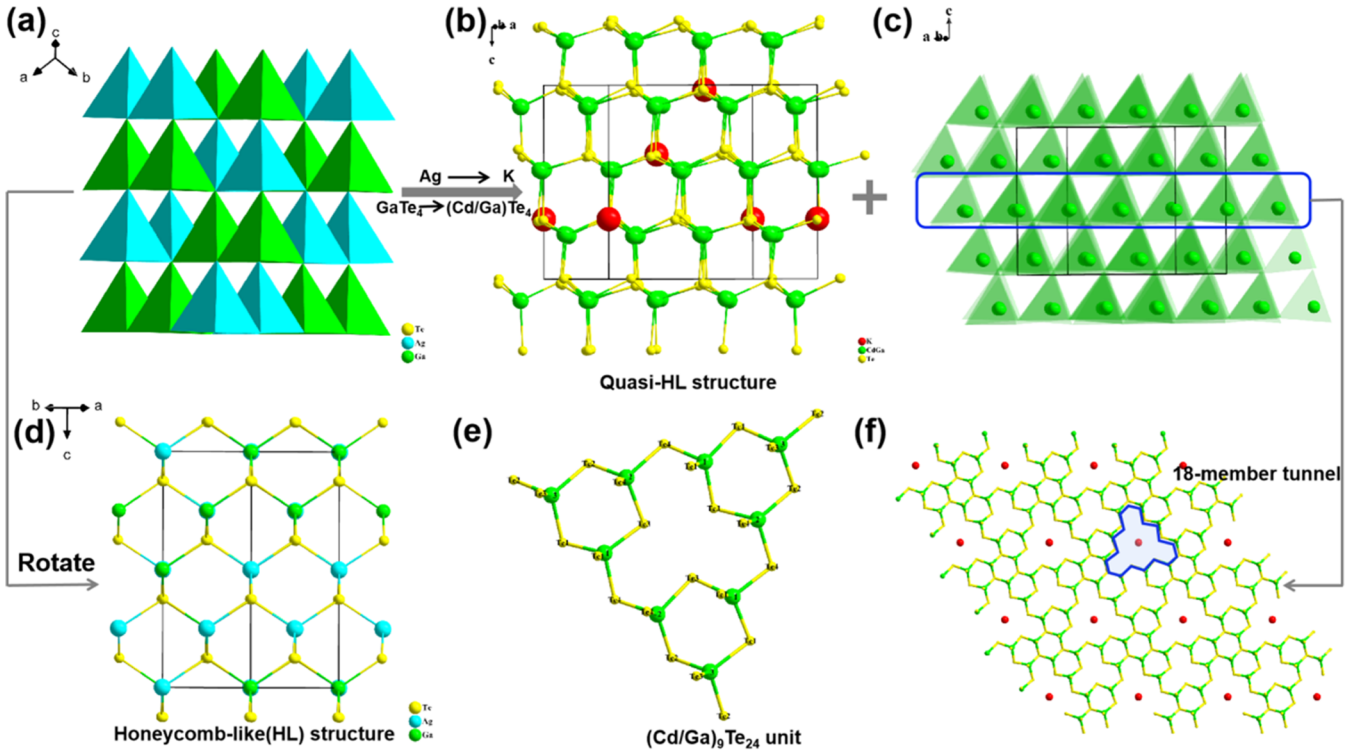


**Figure 2.** (a) Structure of $AgGaTe_2$; (b) quasi-HL structure of $KCd_4Ga_5Te_{12}$; (c) tetrahedron packing of $KCd_4Ga_5Te_{12}$; (d) HL structure of $AgGaTe_2$; (e) asymmetric building unit $(Cd/Ga)_9Te_{24}$; and (f) two-dimensional $[(Cd/Ga)_9Te_{24}]$ layer parallel to the *ab* plane.

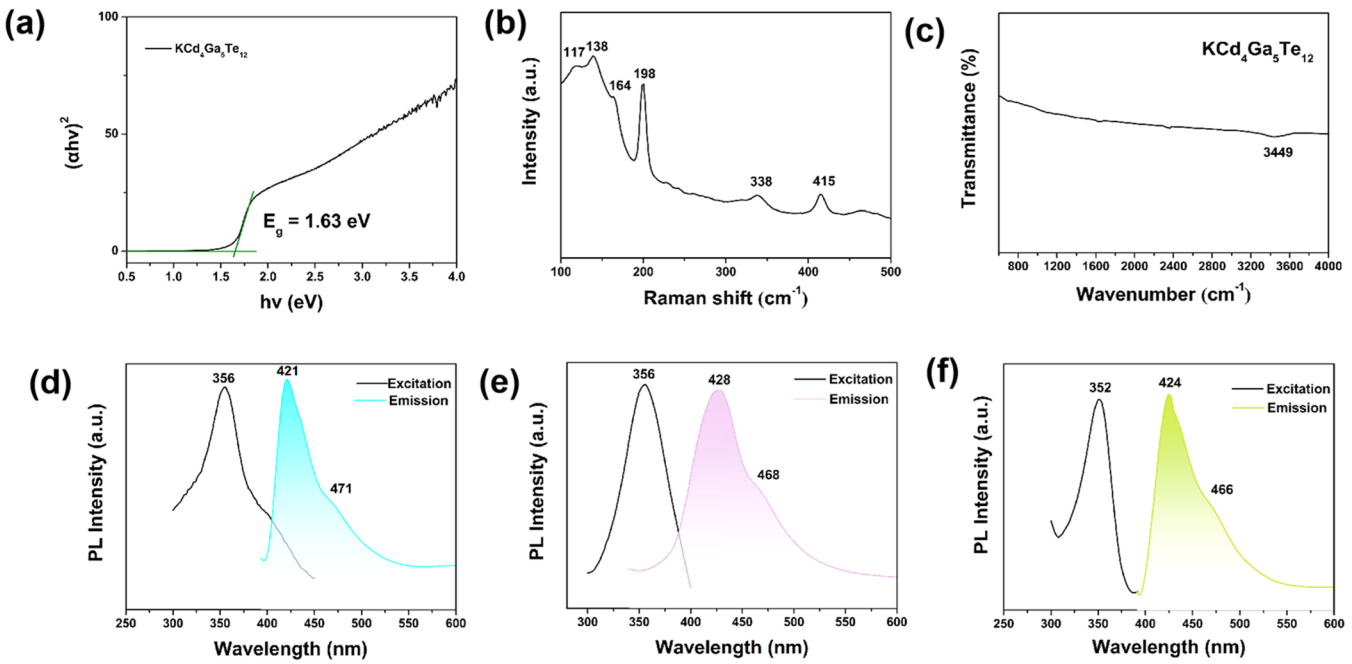


**Figure 3.** (a) UV−vis−NIR diffuse-reflectance spectrum of $KCd_4Ga_5Te_{12}$. Raman (b) and IR spectra (c) of $KCd_4Ga_5Te_{12}$. Solid-state emission and excitation spectra of $KCd_4Ga_5Te_{12}$ (d), $RbCd_4Ga_5Te_{12}$ (e), and $CsCd_4Ga_5Te_{12}$ (f) collected at room temperature.

weighted average values for each atom are calculated, and the results are shown in Table S2. The calculated bond valence sums for all atoms are in good accordance with the expected weighted average values, indicating that the atom assignments are reasonable.

The crystal structure of $KCd_4Ga_5Te_{12}$ is shown in Figure 2. All Cd/Ga atoms are coordinated with four Te atoms to form $(Cd/Ga)Te_4$ tetrahedra with d(Cd/Ga−Te) bond lengths in the range of 2.648(2)−2.762(1) Å and Te−Cd/Ga−Te bond angles in the range of 101.35(5)−121.11(5)°, indicating that these tetrahedra possess relatively large distortion (Figure S5). Then, three $(Cd1/Ga1)Te_4$ tetrahedra, three $(Cd2/Ga2)Te_4$ tetrahedra, and three $(Cd3/Ga3)Te_4$ tetrahedra establish the $(Cd/Ga)_9Te_{24}$ unit through vertex-sharing (Figure 2e). These units are linked to each other to form a two-dimensional $[(Cd/Ga)_9Te_{24}]$ layer parallel to the *ab* plane (Figure 2f), and then


https://doi.org/10.1021/acs.chemmater.3c01493
Chem. Mater. 2023, 35, 7218−7228

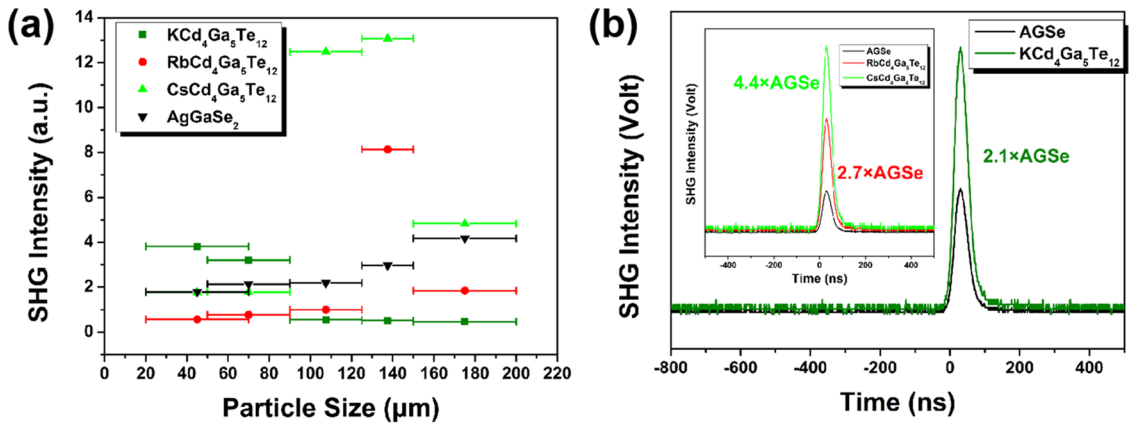


**Figure 4.** (a) Curve of SHG intensity as a function of particle size for $ACd_4Ga_5Te_{12}$ (A = K, Rb, Cs) and AGSe (as reference). (b) Oscilloscope traces of SHG signals of $KCd_4Ga_5Te_{12}$ and AGSe in the particle size range of 20−50 $\mu$m (Inset: Oscilloscope traces of SHG signals of $ACd_4Ga_5Te_{12}$ (A = Rb, Cs) and AGSe in the particle size range of 125−150 $\mu$m).

the layers are stacked along the c-axis to construct an overall three-dimensional framework with $K^+$ filling in the interstitial sites to balance charge (Figure 2b,c). Notably, this structure has an 18-member tunnel perpendicular to the [(Cd/Ga)$_9$Te$_{24}$] layer. The above structural features may endow $KCd_4Ga_5Te_{12}$ with ion exchange ability. In addition, the K atoms are bonded with 12 Te atoms by weak electrostatic interactions with K−Te bond distances ranging from 4.035(8) to 4.121(1) Å (Figure S5d). These K−Te lengths are a little larger than those observed in $K_6CdTe_4$ (3.408(1)−4.083(2) Å).[80] Longer K−Q bonds can also be observed in $KHg_4Ga_5Se_{12}$.[79]

Intriguingly, the structure of $KCd_4Ga_5Te_{12}$ can be seen as evolving from $AgGaTe_2$, which has a chalcopyrite structure. As shown in Figure 2, the covalent frameworks of $AgGaTe_2$ and $KCd_4Ga_5Te_{12}$ are both composed of corner-sharing (Cd/Ga)Te$_4$ tetrahedra. Nevertheless, some obvious structural evolution processes can be summarized. On the one hand, $Ag^+$ is replaced by alkali metal $K^+$ with a larger ionic radius, resulting in K occupying one of the Te positions, which makes the arrangement of Te atoms no longer the closest packing manner. On the other hand, the Ga sites are substituted by the coexisting multivalent metal positions of Cd and Ga, replacing the 3D honeycomb-like (HL) structure composed of AgTe$_4$ and GaTe$_4$ tetrahedra connected by shared corners along the *c*-axis (Figure 2a,d) with a quasi-HL framework structure consisting of (Cd/Ga)Te$_4$ tetrahedra interconnected with certain alignment deviations (Figure 2b). Therefore, selecting $AgGaTe_2$ as the template and introducing alkali metal and multivalent metal into the crystal structure affords the discovery of NLO telluride with a flexible structure and favorable properties.

**Optical Properties.** The UV−vis−NIR diffuse-reflectance spectrum, Raman, and IR spectra of $KCd_4Ga_5Te_{12}$ are given in Figure 3. The optical band gap is deduced by the Tauc plot method.[81] The result indicates that the band gap of $KCd_4Ga_5Te_{12}$ is about 1.63 eV, which is consistent with its gray color. Furthermore, it is worth noting that there is little light absorption below the band gap, indicating that the high purity of the polycrystalline sample and the light transmission on the title compound are not disturbed (Figure 3a). In addition, the UV−vis−NIR diffuse-reflectance spectra of $RbCd_4Ga_5Te_{12}$ and $CsCd_4Ga_5Te_{12}$ are shown in Figure S6. The results indicate that their band gaps are 1.41 and 1.53 eV, respectively. Such band gaps are close to those of AGSe and ZGP, which makes the material suitable for ordinary 2 $\mu$m lasers that serve as the pump source for IR laser generation. The Raman spectra of the title compounds are exhibited in Figures 3b and S7. The little difference in Raman spectra between the three compounds can be attributed to their similar structures. Several absorption peaks appeared from 100 to 500 cm$^{-1}$. The most obvious Raman shift at 198 cm$^{-1}$ can be assigned to the symmetric stretch of Cd−Te bonds, which corresponds well with the 195 cm$^{-1}$ peak observed in $CdGa_2Te_4$.[82] The peaks at 338 and 415 cm$^{-1}$ are attributed to Ga−Te vibration modes, and it agrees well with the fact that the lighter weight of an atom always results in a higher stretching wavenumber.[79] The other peaks below 200 cm$^{-1}$ might come from the A−Te vibrations.[83,84] The IR spectra of the title compounds are given in Figures 3c and S8. Notably, the short-wave cutoff has not been identified due to the too-small single crystals, which are obtained by the spontaneous crystallization method. Nevertheless, the IR spectrum indicates that the transparent range of $ACd_4Ga_5Te_{12}$ (A = K, Rb, Cs) is up to 25 $\mu$m because there is no significant absorption peak (the peaks located at about 3450 cm$^{-1}$ are caused by vibrations in the O−H bond in $H_2O$), which is significantly wider than those of sulfides and selenides.[61] It is worth noting that the search for NLO materials in the far IR or even the terahertz range is becoming increasingly important.

The excitation and emission spectra of $ACd_4Ga_5Te_{12}$ are shown in Figure 3d−f. The title compounds display a strong emission band centered at 421−428 nm, accompanied by a weaker emission band centered at 466−471 nm at room temperature, with an excitation maximum at 352−356 nm. The strong fluorescence emissions at 421−428 nm are believed to be caused by the existence of point defects in the structures, which may become electron trapping centers, resulting in a high electron−hole pair recombination rate.[77,85] The weak luminescence at 466−471 nm can be attributed to exciton luminescence caused by exciton recombination because the $d^{10}$ configuration of $Cd^{2+}$ makes it difficult to carry out electron transfer.[86] In addition, a study has illustrated the existence of Cd atoms has an important effect on the increase of triplet-state radiative rate.[87] Due to exciton phonon coupling, the Stokes shifts of $ACd_4Ga_5Te_{12}$ (A = K, Rb, Cs) are 65, 72, and 72 nm, respectively. The appropriate Stokes shifts indicate the potential of the title compounds as luminescent materials. This


https://doi.org/10.1021/acs.chemmater.3c01493
Chem. Mater. 2023, 35, 7218−7228

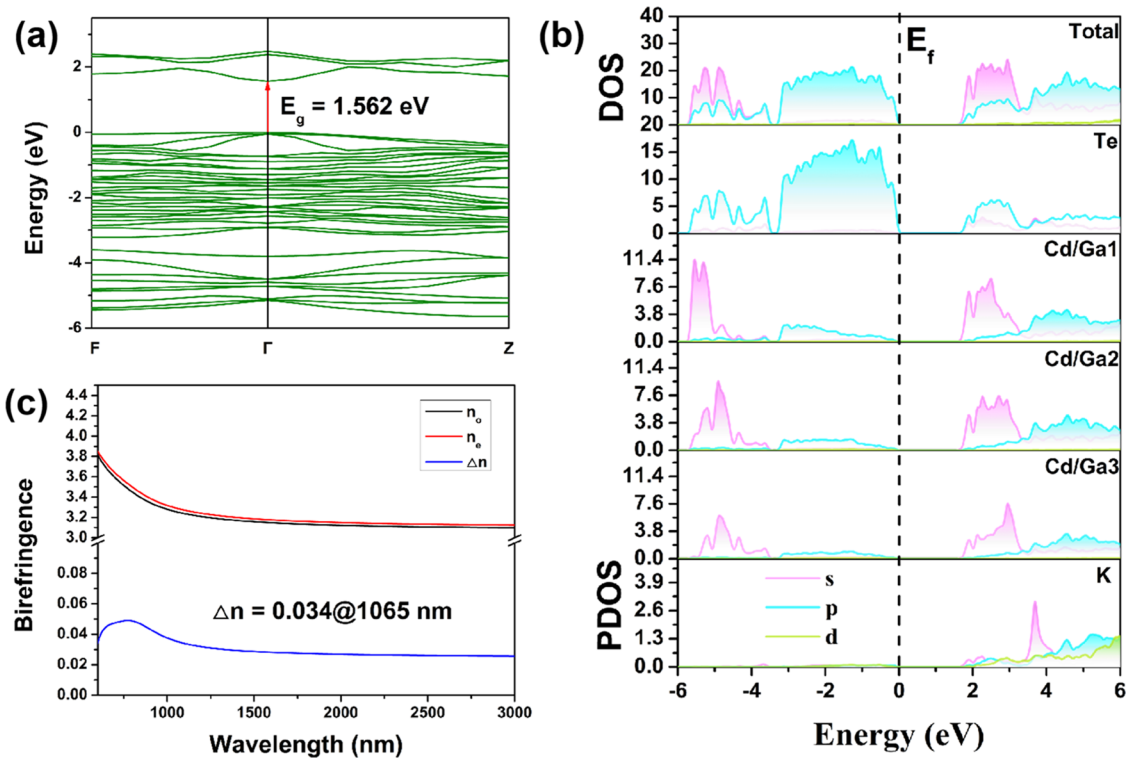


**Figure 5.** (a) Calculated band structure of $KCd_4Ga_5Te_{12}$. (b) Total and partial densities of states of $KCd_4Ga_5Te_{12}$. (c) Dispersion curve of the refractive index with the wavelength.

may be because a larger Stokes shift results in greater absorbed energy loss and less energy used for luminescence, while a smaller Stokes shift can easily lead to severe self-absorption and is not conducive to luminescence. Furthermore, strong photoluminescence is usually found in chalcogenides, such as gallium sulfides with 440−500 nm luminescence,[88] $CdGa_2S_4$ with 577 nm luminescence,[89] $ACd_4Ga_5S_{12}$ (A = K, Rb, Cs) with 574−595 nm luminescence,[77] and $Ba_3AGa_5Se_{10}Cl_2$ (A = Cs, Rb, K) with 711−731 nm luminescence outputs.[90] It is rare to observe the 421−428 nm luminescence output in chalcogenides, extending the emission region of chalcogenides photoluminescence.

**SHG Properties.** The powder NLO properties of the title compounds were investigated using the Kurtz−Perry method with a Q-switched Ho:Tm:Cr:YAG laser (2.09 $\mu$m, 1 Hz, 100 ns). The curves of SHG intensity as a function of particle size for $ACd_4Ga_5Te_{12}$ (A = K, Rb, Cs) and AGSe (as reference) are shown in Figure 4a. The results indicate the type-I nonphase-matchable nature of the title compounds at 2090 nm. Specifically, the SHG response of $KCd_4Ga_5Te_{12}$ decreases gradually with the increase of particle size, while the SHG intensities of Rb and CS compounds first increase with the increasing particle size and then decrease when the particle size reaches 125−150 $\mu$m. Therefore, $KCd_4Ga_5Te_{12}$ reaches the maximum SHG response with the particle size of 20−50 $\mu$m, while $RbCd_4Ga_5Te_{12}$ and $CsCd_4Ga_5Te_{12}$ realize their SHG intensity maxima at the particle size of 125−150 $\mu$m. Furthermore, the SHG response of $KCd_4Ga_5Te_{12}$ is about 2.1 times that of the commercial material AGSe if compared in the same particle size range of 20−50 $\mu$m (Figure 4b). Similarly, the relative SHG intensities of Rb and Cs compounds are approximately 2.7 and 4.4 times that of AGSe at the 125−150 $\mu$m particle size, respectively (Figure 4b inset). To the best of our knowledge, these values are larger than most reported nonphase-matching tellurides; some examples are $CsMn_4In_5Te_{12}$, 1.7 × AGS; $CsZn_4In_5Te_{12}$, 4.3 × AGS; $CsCd_4In_5Te_{12}$, 9.2 × AGS; and $Ba_2Ge_2Te_5$, 0.45 × AGS.[76,91] Moreover, the measured optical properties of the $AM_4^{II}M_5^{III}Q_{12}$ (A = K−Cs; $M^{II}$ = $Mn^{2+}$, $Zn^{2+}$, $Cd^{2+}$, $Hg^{2+}$; $M^{III}$ = $Ga^{3+}$, $In^{3+}$; Q = S, Se, Te) family are summarized in Table S7. It is clear that all members except $KHg_4Ga_5Se_{12}$ exhibit nonphase-matching behavior. This may be because the introduction of the Hg atom increases the optical anisotropy, which sheds light on the exploration of phase-matching materials in this family.

**Theoretical Studies.** In order to analyze the in-depth mechanism of the optical properties of $KCd_4Ga_5Te_{12}$, detailed theoretical calculations using the CASTEP package were performed. The band structure calculation indicates that the direct band gap of $KCd_4Ga_5Te_{12}$ is 1.562 eV, which is close to the measured gap value of 1.63 eV (Figure 5a). Therefore, no scissor correction was needed in evaluating linear and nonlinear optical properties. Furthermore, the density of states (DOS) and partial DOS projected on constitutional atoms are demonstrated in Figure 5b. The results show that the two sides of the band gap are dominated by Te nonbonding p orbitals at occupied bands, and the contributions of the three kinds of Cd/Ga to DOS are almost indistinguishable. The edges of unoccupied bands mostly consist of s and p orbitals of Cd, Ga, and Te ions. It is expected that K does not play a role in optical properties in terms of direct electronic transition. After optical property calculations, we can obtain the refractive indices; the optical axis is found to be the $z$-axis, as the model indicates in Figure S9. The calculated dispersive refractive indices are exhibited in Figure 5c, and it is revealed that $KCd_4Ga_5Te_{12}$ is a positive uniaxial crystal with $n_e \geq n_o$. The static birefringence of


https://doi.org/10.1021/acs.chemmater.3c01493
Chem. Mater. 2023, 35, 7218−7228

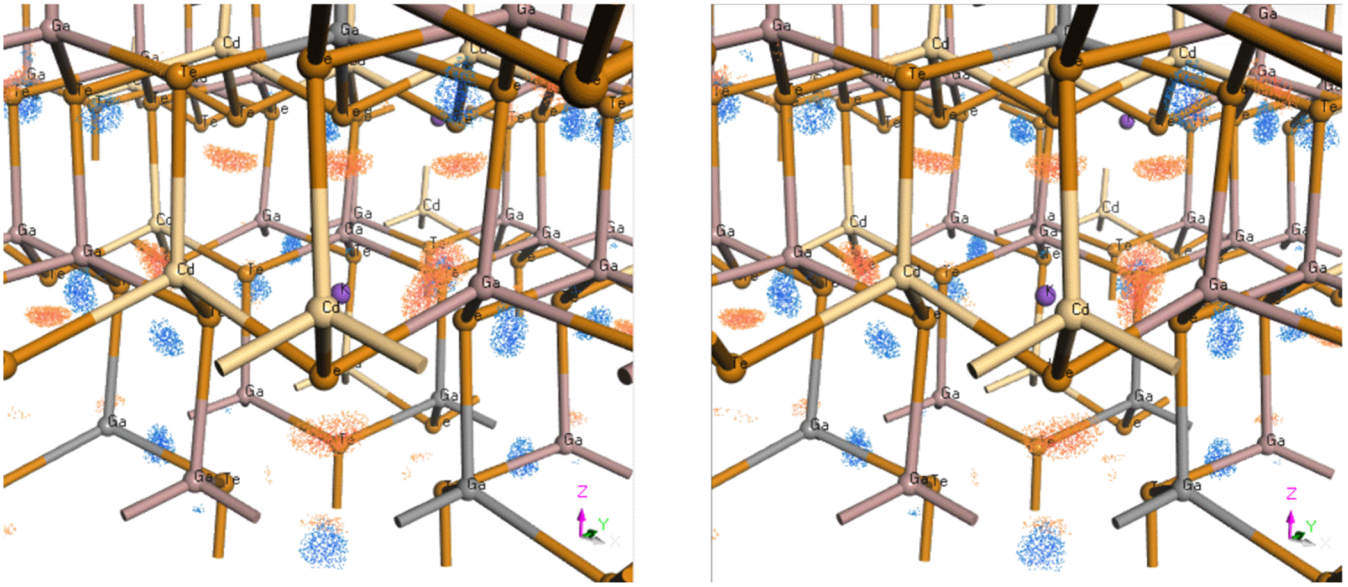

**Figure 6.** Side view of cross-eyed stereo pairs of $\chi_{333}^{(2)}$ SHG densities of both VE occupied (VE occ) (orange) and VH unoccupied (VH unocc) (blue) processes displayed in the same figure.

$KCd_4Ga_5Te_{12}$ is 0.034@1065 nm. The relatively small $\Delta n$ values in the IR region indicate nonphase-matchable behaviors, which are consistent with the experimental observations. Incidentally, if the standard CASTEP 2017R2 set of the pseudopotential library is used and the same $E_{tot}$ vs $E_{cut}$ convergence tolerance is set to 0.1 eV/atom (i.e., the "Fine" quality according to the Materials Studio interface), the $E_{cut}$ will be 435 eV and the calculated band gap will be 1.079 eV, which means 0.551 eV should be used as a scissor shift. We have performed such calculations and obtained the calculated birefringence to be 0.0355@1065 nm ($n_e$ = 3.29175, $n_o$ = 3.25625).

As restricted by the Kleinman symmetry rules, $KCd_4Ga_5Te_{12}$ possesses four non-zero independent second-order polarizability tensors ($\chi_{111}^{(2)}$, $\chi_{113}^{(2)}$, $\chi_{222}^{(2)}$, $\chi_{333}^{(2)}$) due to its $R3$ space group. Accordingly, the SHG coefficients $d_{11}$, $d_{15}$, $d_{22}$, and $d_{33}$ corresponding to these tensors are calculated as below: $d_{11}$ = 8.407 pm/V, $d_{15}$ = −8.276 pm/V, $d_{22}$ = −6.932 pm/V, and $d_{33}$ = 13.908 pm/V. It is worth noting that the calculated $d_{33}$ value is closest to the SHG response at the maximum particle size rather than the largest SHG intensity.[92] Correspondingly, the SHG response of $KCd_4Ga_5Te_{12}$ is about 0.1 times that of AGSe in the particle size range of 150−200 $\mu$m, which is in good agreement with the theoretical results. Similar to birefringence calculations, ultrasoft pseudopotentials are also used to calculate SHG coefficients, and $d_{33}$ is 13.5 pm/V. Both birefringence and $d_{33}$ are consistent with the calculations using the harder set of norm-conserving pseudopotentials. CASTEP implemented in VCA works for both pseudopotential types, as can be demonstrated in the present study. In addition, geometry optimization with fully relaxed cell size and shape was also performed (with symmetry kept), and the cell volume increased by about 6% (cell parameters were enlarged by 2.1%). Band gap, birefringence, and nonlinear optical coefficients are basically unchanged.

The origin of SHG is discussed by means of SHG density. The cross-eyed stereo pair of the crystal structure of $KCd_4Ga_5Te_{12}$ is given in Figure S10. Herein, the occupied and unoccupied states subsystem contributions of SHG are best represented by the VE occupied (VE occ) and VH unoccupied (VH unocc) orbitals, respectively. Here, we plot the VE occ in the reverse rainbow color scheme (high-value red) and the VH unocc in the normal rainbow color scheme (high-value blue). In parallel, the SHG "hot spots" (of $\chi_{333}^{(2)}$) in $KCd_4Ga_5Te_{12}$ are visualized in a compact way in the cross-eyed stereo-pair images shown in Figures 6 and S11. All SHG densities originate from Te ions, and electron lone-pair density obviously plays an important role in occupied SHG densities. First, a very strong SHG effect comes from clustered triple contiguous Te tips parallelly pointing downward to the -$z$ direction; they all connected two Cd/Ga3 ions and one Cd/Ga2 ions. These contribute to VE occ SHG density only. Here, we call them type-I Te. Second, the Te ions located above the Cd/Ga2 ion have a lone-pair cap pointing 45 degrees; these contribute both VE occ (obviously lone-pair electrons) and VH unocc (anticap site); here, we call them type-II Te. Finally, the Te atoms located above Cd/Ga1 ions (which are also connected to another Cd/Ga1 ion and one Cd/Ga3 ion) are only active for VH unocc, and here, we call them type-III Te. In general, the occupied state SHG contribution comes from lone-pair electrons of type-I and type-II Te, whereas empty states of SHG consist of type-II and type-III Te. The local structure of $KCd_4Ga_5Te_{12}$ was placed in Figure S12 to conveniently indicate the type of Te in its SHG function.

## CONCLUSIONS

In summary, three non-centrosymmetric quaternary tellurides, $ACd_4Ga_5Te_{12}$ (A = K, Rb, Cs), were synthesized and characterized. Although $KCd_4Ga_5Te_{12}$ and its structural prototype $AgGaTe_2$ possess similar covalent structures, the cation occupancies and the detailed stacking modes of the basic motifs differ greatly in these two compounds. The three-dimensional framework of $ACd_4Ga_5Te_{12}$ is built by corner-sharing $Cd/GaTe_4$ tetrahedra with discrete A ions filling in the interstitial sites. For these compounds, it is very interesting that all of the NLO-active units are arranged in a completely noncancelling manner, which facilitates the enhancement of SHG effects. Therefore, their SHG responses were determined


https://doi.org/10.1021/acs.chemmater.3c01493
Chem. Mater. 2023, 35, 7218−7228

for the first time, and they are approximately 2.1, 2.7, and 4.4 times that of commercial AGSe in the particle size range of 20−50 (125−150) $\mu$m, respectively. The SHG-density analysis reveals that the largest component $\chi_{333}^{(2)}$ of $KCd_4Ga_5Te_{12}$ originates from three types of Te in the crystal structure. This study proves that the CASTEP implemented in VCA is suitable for two types of norm-conserving and ultrasoft pseudopotentials. Furthermore, title compounds also exhibit strong photoluminescence properties at 298 K. Besides, $ACd_4Ga_5Te_{12}$ possesses moderate band gaps and a wide transmission range, implying that they are promising candidates in the IR NLO applications. More importantly, outstanding crystal engineering creating noncancelling frameworks to enhance optical nonlinearity (such as type-I Te) can be realized by naturally site-occupancy disordered crystals. This strategy opens up a new direction for the search and design of NLO crystals.

## ■ ASSOCIATED CONTENT

### Supporting Information

The Supporting Information is available free of charge at https://pubs.acs.org/doi/10.1021/acs.chemmater.3c01493.

CIF data and atomic coordinates ($\times 10^4$); equivalent isotropic displacement parameters; selected bond lengths (Å) and sngles (°) for $KCd_4Ga_5Te_{12}$; results of the Rietveld refinement for $RbCd_4Ga_5Te_{12}$ and $CsCd_4Ga_5Te_{12}$; bonds lengths and angles of $RbCd_4Ga_5Te_{12}$ and $CsCd_4Ga_5Te_{12}$; powder X-ray diffraction; and EDX result of $KCd_4Ga_5Te_{12}$, $RbCd_4Ga_5Te_{12}$, and $CsCd_4Ga_5Te_{12}$ (PDF)

### Accession Codes

CCDC 2268523 contains the supplementary crystallographic data for this paper.

## ■ AUTHOR INFORMATION


### Corresponding Authors

**Ming-Hsien Lee** − *Department of Physics, Tamkang University, New Tapei 25137, Taiwan;* orcid.org/0000-0003-3956-181X; Email: mhslee@mail.tku.edu.tw

**Jiyong Yao** − *Beijing Center for Crystal Research and Development, Key Lab of Functional Crystals and Laser Technology, Technical Institute of Physics and Chemistry, Chinese Academy of Sciences, Beijing 100190, P. R. China; Center of Materials Science and Optoelectronics Engineering, University of Chinese Academy of Sciences, Beijing 100049, P. R. China;* orcid.org/0000-0002-4802-5093; Email: jyao@mail.ipc.ac.cn

### Authors

**Mengran Sun** − *Beijing Center for Crystal Research and Development, Key Lab of Functional Crystals and Laser Technology, Technical Institute of Physics and Chemistry, Chinese Academy of Sciences, Beijing 100190, P. R. China; Center of Materials Science and Optoelectronics Engineering, University of Chinese Academy of Sciences, Beijing 100049, P. R. China*

**Wenhao Xing** − *Institute of Chemical Materials, China Academy of Engineering Physics, Mianyang 621900, P. R. China;* orcid.org/0000-0003-1258-419X

**Shyong K. Chen** − *Department of Physics, Tamkang University, New Tapei 25137, Taiwan*

**Chunxiao Li** − *Beijing Center for Crystal Research and Development, Key Lab of Functional Crystals and Laser Technology, Technical Institute of Physics and Chemistry, Chinese Academy of Sciences, Beijing 100190, P. R. China; Center of Materials Science and Optoelectronics Engineering, University of Chinese Academy of Sciences, Beijing 100049, P. R. China*

**Wenhao Liu** − *Beijing Center for Crystal Research and Development, Key Lab of Functional Crystals and Laser Technology, Technical Institute of Physics and Chemistry, Chinese Academy of Sciences, Beijing 100190, P. R. China; Center of Materials Science and Optoelectronics Engineering, University of Chinese Academy of Sciences, Beijing 100049, P. R. China*

Complete contact information is available at: https://pubs.acs.org/10.1021/acs.chemmater.3c01493


### Notes

The authors declare no competing financial interest.

## ■ ACKNOWLEDGMENTS

This research was supported by the National Natural Science Foundation of China (22175190, 51890862).

## ■ REFERENCES


(1) Eaton, D. F. Nonlinear Optical Materials. *Science* **1991**, *253*, 281−287.

(2) Keller, U. Recent developments in compact ultrafast lasers. *Nature* **2003**, *424*, 831−838.

(3) Halasyamani, P. S.; Rondinelli, J. M. The must-have and nice-to-have experimental and computational requirements for functional frequency doubling deep-UV crystals. *Nat. Commun.* **2018**, *9*, No. 2972.

(4) Li, Y.; Luo, J.; Zhao, S. Local Polarity-Induced Assembly of Second-Order Nonlinear Optical Materials. *Acc. Chem. Res.* **2022**, *55*, 3460−3469.

(5) Wu, C.; Yang, G.; Humphrey, M. G.; Zhang, C. Recent advances in ultraviolet and deep-ultraviolet second-order nonlinear optical crystals. *Coord. Chem. Rev.* **2018**, *375*, 459−488.

(6) Gong, P.; Liang, F.; Kang, L.; Chen, X.; Qin, J.; Wu, Y.; Lin, Z. Recent advances and future perspectives on infrared nonlinear optical metal halides. *Coord. Chem. Rev.* **2019**, *380*, 83−102.

(7) Pan, Y.; Guo, S.-P.; Liu, B.-W.; Xue, H.-G.; Guo, G.-C. Second-order nonlinear optical crystals with mixed anions. *Coord. Chem. Rev.* **2018**, *374*, 464−496.

(8) Guo, S.-P.; Chi, Y.; Guo, G.-C. Recent achievements on middle and far-infrared second-order nonlinear optical materials. *Coord. Chem. Rev.* **2017**, *335*, 44−57.

(9) Chung, I.; Kanatzidis, M. G. Metal Chalcogenides: A Rich Source of Nonlinear Optical Materials. *Chem. Mater.* **2014**, *26*, 849−869.

(10) Li, Z.; Zhang, S.; Huang, Z.; Zhao, L.-D.; Uykur, E.; Xing, W.; Lin, Z.; Yao, J.; Wu, Y. Molecular Construction from $AgGaS_2$ to $CuZnPS_4$: Defect-Induced Second Harmonic Generation Enhancement and Cosubstitution-Driven Band Gap Enlargement. *Chem. Mater.* **2020**, *32*, 3288−3296.

(11) Guo, Y.; Liang, F.; Yin, W.; Li, Z.; Luo, X.; Lin, Z.-S.; Yao, J.; Mar, A.; Wu, Y. $BaHgGeSe_4$ and $SrHgGeSe_4$: Two New Hg-Based Infrared Nonlinear Optical Materials. *Chem. Mater.* **2019**, *31*, 3034−3040.

(12) Luo, X.; Li, Z.; Guo, Y.; Yao, J.; Wu, Y. Recent progress on new infrared nonlinear optical materials with application prospect. *J. Solid State Chem* **2019**, *270*, 674−687.

(13) Kang, L.; Lin, Z. Deep-ultraviolet nonlinear optical crystals: concept development and materials discovery. *Light: Sci. Appl.* **2022**, *11*, No. 201.

(14) Li, Y.-Y.; Wang, W.-J.; Wang, H.; Lin, H.; Wu, L.-M. Mixed-Anion Inorganic Compounds: A Favorable Candidate for Infrared Nonlinear Optical Materials. *Cryst. Growth Des.* **2019**, *19*, 4172−4192.
(15) Yang, H.-D.; Ran, M.-Y.; Wei, W.-B.; Wu, X.-T.; Lin, H.; Zhu, Q.-L. Recent advances in IR nonlinear optical chalcogenides with well-balanced comprehensive performance. *Mater. Today Phys.* **2023**, *35*, No. 101127.
(16) Wang, P.; Chu, Y.; Tudi, A.; Xie, C.; Yang, Z.; Pan, S.; Li, J. The Combination of Structure Prediction and Experiment for the Exploration of Alkali-Earth Metal-Contained Chalcopyrite-Like IR Nonlinear Optical Material. *Adv. Sci.* **2022**, *9*, No. 2106120.
(17) Chen, H.; Wei, W.-B.; Lin, H.; Wu, X.-T. Transition-metal-based chalcogenides: A rich source of infrared nonlinear optical materials. *Coord. Chem. Rev.* **2021**, *448*, No. 214154.
(18) Reshak, A. H.; Atuchin, V. V.; Auluck, S.; Kityk, I. V. First and second harmonic generation of the optical susceptibilities for the non-centro-symmetric orthorhombic $AgCd_2GaS_4$. *J. Phys.: Condens. Matter* **2008**, *20*, No. 325234.
(19) Shevchuk, M. V.; Atuchin, V. V.; Kityk, A. V.; Fedorchuk, A. O.; Romanyuk, Y. E.; CaŁus, S.; Yurchenko, O. M.; Parasyuk, O. V. Single crystal preparation and properties of the $AgGaGeS_4$−$AgGaGe_3Se_8$ solid solution. *J. Cryst. Growth* **2011**, *318*, 708−712.
(20) Atuchin, V. V.; Liang, F.; Grazhdannikov, S.; Isaenko, L. I.; Krinitsin, P. G.; Molokeev, M. S.; Prosvirin, I. P.; Jiang, X.; Lin, Z. Negative thermal expansion and electronic structure variation of chalcopyrite type $LiGaTe_2$. *RSC Adv.* **2018**, *8*, 9946−9955.
(21) Chemla, D.; Kupecek, P.; Robertson, D.; Smith, R. Silver thiogallate, a new material with potential for infrared devices. *Opt. Commun.* **1971**, *3*, 29−31.
(22) Boyd, G.; Kasper, H.; McFee, J.; Storz, F. Linear and nonlinear optical properties of some ternary selenides. *IEEE J. Quantum Electron.* **1972**, *8*, 900−908.
(23) Boyd, G. D.; Buehler, E.; Storz, F. Linear and nonlinear optical properties of $ZnGeP_2$ and CdSe. *Appl. Phys. Lett.* **1971**, *18*, 301−304.
(24) Feng, Z.-S.; Kang, Z.-H.; Wu, F.-G.; Gao, J.-Y.; Jiang, Y.; Zhang, H.-Z.; Andreev, Y. M.; Lanskii, G. V.; Atuchin, V. V.; Gavrilova, T. A. SHG in doped GaSe:In crystals. *Opt. Express* **2008**, *16*, 9978−9985.
(25) Atuchin, V. V.; Lin, Z. S.; Isaenko, L. I.; Kesler, V. G.; Kruchinin, V. N.; Lobanov, S. I. Optical properties of $LiGaS_2$: an ab initio study and spectroscopic ellipsometry measurement. *J. Phys.: Condens. Matter* **2009**, *21*, No. 455502.
(26) Kamijoh, T.; Kuriyama, K. Single crystal growth and characterization of LiInSe2. *J. Cryst. Growth* **1981**, *51*, 6−10.
(27) Wang, Y.; Tikhonov, E.; Niu, H. Prediction of Promising Deep Ultraviolet Nonlinear Optical Materials in the $Li_2O$−$B_2O_3$ System. *Chem. Mater.* **2023**, *35*, 4201−4210.
(28) Mutailipu, M.; Pan, S. Emergent Deep-Ultraviolet Nonlinear Optical Candidates. *Angew. Chem., Int. Ed.* **2020**, *59*, 20302−20317.
(29) Lin, H.; Wei, W.-B.; Chen, H.; Wu, X.-T.; Zhu, Q.-L. Rational design of infrared nonlinear optical chalcogenides by chemical substitution. *Coord. Chem. Rev.* **2020**, *406*, No. 213150.
(30) Li, J.; Yao, W.-D.; Li, J.-N.; Li, X.-H.; Liu, W.; Guo, S.-P. Partial substitution induced structural transformation and enhanced nonlinear optical properties of $Na_2Ga_xIn_{6-x}Se_{10}$ (x = 3, 3.76). *Mater. Today Phys.* **2023**, *32*, No. 101007.
(31) Ran, M.-Y.; Wang, A. Y.; Wei, W.-B.; Wu, X.-T.; Lin, H.; Zhu, Q.-L. Recent progress in the design of IR nonlinear optical materials by partial chemical substitution: Structural evolution and performance optimization. *Coord. Chem. Rev.* **2023**, *481*, No. 215059.
(32) Wu, M.; Tikhonov, E.; Tudi, A.; Kruglov, I.; Hou, X.; Xie, C.; Pan, S.; Yang, Z. Target-Driven Design of Deep-UV Nonlinear Optical Materials via Interpretable Machine Learning. *Adv. Mater.* **2023**, *35*, No. 2300848.
(33) Hu, C.-L.; Han, Y.-X.; Fang, Z.; Mao, J.-G. $Zn_2BS_3Br$: An Infrared Nonlinear Optical Material with Significant Dual-Property Enhancements Designed through a Template Grafting Strategy. *Chem. Mater.* **2023**, *35*, 2647−2654.
(34) Xing, W.; Wang, N.; Tang, C.; Li, C.; Lin, Z.; Yao, J.; Yin, W.; Kang, B. From $AgGaS_2$ to $AgHgPS_4$: vacancy defects and highly distorted $HgS_4$ tetrahedra double-induced remarkable second-harmonic generation response. *J. Mater. Chem. C* **2021**, *9*, 1062−1068.
(35) Li, R.-A.; Liu, Q.-Q.; Liu, X.; Liu, Y.; Jiang, X.; Lin, Z.; Jia, F.; Xiong, L.; Chen, L.; Wu, L.-M. $Na_2Ba[Na_2Sn_2S_7]$: Structural Tolerance Factor-Guided NLO Performance Improvement. *Angew. Chem., Int. Ed.* **2023**, *62*, No. e202218048.
(36) Sun, M.; Xing, W.; Lee, M.-H.; Yao, J. Bridging oxygen atoms in trigonal prism units driven strong second-harmonic-generation efficiency in $Sr_3Ge_2O_4Te_3$. *Chem. Commun.* **2022**, *58*, 11167−11170.
(37) Li, J.-N.; Yao, W.-D.; Li, X.-H.; Liu, W.; Xue, H.-G.; Guo, S.-P. A novel promising infrared nonlinear optical selenide $KAg_3Ga_8Se_{14}$ designed from benchmark $AgGaQ_2$ (Q = S, Se). *Chem. Commun.* **2021**, *57*, 1109−1112.
(38) Li, Y.-N.; Chi, Y.; Sun, Z.-D.; Xue, H.; Suen, N.-T.; Guo, S.-P. Partial substitution induced centrosymmetric to noncentrosymmetric structure transformation and promising second-order nonlinear optical properties of $(K_{0.38}Ba_{0.81})Ga_2Se_4$. *Chem. Commun.* **2019**, *55*, 13701−13704.
(39) Hou, Y.; Wu, H.; Yu, H.; Hu, Z.; Wang, J.; Wu, Y. An Effective Strategy for Designing Nonlinear Optical Crystals by Combining the Structure-Directing Property of Oxyfluorides with Chemical Substitution. *Angew. Chem., Int. Ed.* **2021**, *60*, 25302−25306.
(40) Andreev, Y. M.; Atuchin, V. V.; Lanskii, G. V.; Pervukhina, N. V.; Popov, V. V.; Trocenco, N. C. Linear optical properties of $LiIn(S_{1-x}Se_x)_2$ crystals and tuning of phase matching conditions. *Solid State Sci.* **2005**, *7*, 1188−1193.
(41) Sachanyuk, V. P.; Gorgut, G. P.; Atuchin, V. V.; Olekseyuk, I. D.; Parasyuk, O. V. The $Ag_2S$−$In_2S_3$−$Si(Ge)S_2$ systems and crystal structure of quaternary sulfides $Ag_2In_2Si(Ge)S_6$. *J. Alloys Compd.* **2008**, *452*, 348−358.
(42) Wang, J.; Wu, H.; Yu, H.; Hu, Z.; Wang, J.; Wu, Y. $Pb_4SeBr_6$: A Congruently Melting Mid-Infrared Nonlinear Optical Material with Excellent Comprehensive Performance. *Adv. Opt. Mater.* **2022**, *10*, No. 2102673.
(43) Yang, H.-D.; Ran, M.-Y.; Zhou, S.-H.; Wu, X.-T.; Lin, H.; Zhu, Q.-L. Rational design via dual-site aliovalent substitution leads to an outstanding IR nonlinear optical material with well-balanced comprehensive properties. *Chem. Sci.* **2022**, *13*, 10725−10733.
(44) Li, X.-H.; Shi, Z.-H.; Yang, M.; Liu, W.; Guo, S.-P. $Sn_7Br_{10}S_2$: The First Ternary Halogen-Rich Chalcohalide Exhibiting a Chiral Structure and Pronounced Nonlinear Optical Properties. *Angew. Chem., Int. Ed.* **2022**, *61*, No. e202115871.
(45) Liu, B.-W.; Jiang, X.-M.; Zeng, H.-Y.; Guo, G.-C. $[ABa_2Cl]$-$[Ga_4S_8]$ (A = Rb, Cs): Wide-Spectrum Nonlinear Optical Materials Obtained by Polycation-Substitution-Induced Nonlinear Optical (NLO)-Functional Motif Ordering. *J. Am. Chem. Soc.* **2020**, *142*, 10641−10645.
(46) Sun, M.; Zhang, X.; Li, C.; Liu, W.; Lin, Z.; Yao, J. Highly polarized $[GeOTe_3]$ motif-driven structural order promotion and an enhanced second harmonic generation response in the new nonlinear optical oxytelluride $Ba_3Ge_2O_4Te_3$. *J. Mater. Chem. C* **2021**, *10*, 150−159.
(47) Chu, Y.; Wang, P.; Zeng, H.; Cheng, S.; Su, X.; Yang, Z.; Li, J.; Pan, S. $Hg_3P_2S_8$: A New Promising Infrared Nonlinear Optical Material with a Large Second-Harmonic Generation and a High Laser-Induced Damage Threshold. *Chem. Mater.* **2021**, *33*, 6514−6521.
(48) Li, Z.; Yao, J.; Wu, Y. Chalcophosphates: A Treasure House of Infrared Nonlinear Optical Materials. *Cryst. Growth Des.* **2020**, *20*, 7550−7564.
(49) Liang, F.; Kang, L.; Lin, Z.; Wu, Y.; Chen, C. Analysis and prediction of mid-IR nonlinear optical metal sulfides with diamond-like structures. *Coord. Chem. Rev.* **2017**, *333*, 57−70.
(50) Wu, K.; Pan, S. $Li_2HgMS_4$ (M = Si, Ge, Sn): New Quaternary Diamond-Like Semiconductors for Infrared Laser Frequency Conversion. *Crystals* **2017**, *7*, 107.

(51) Eifler, A.; Riede, V.; Brückner, J.; Weise, S.; Krämer, V.; Lippold, G.; Schmitz, W.; Bente, K.; Grill, W. Band Gap Energies and Lattice Vibrations of the Lithium Ternary Compounds $LiInSe_2$, $LiInS_2$, $LiGaSe_2$ and $LiGaS_2$. *Jpn. J. Appl. Phys.* **2000**, *39*, 279.
(52) Reshak, A. H.; Auluck, S.; Piasecki, M.; Myronchuk, G. L.; Parasyuk, O.; Kityk, I. V.; Kamarudin, H. Absorption and photoconductivity spectra of $Ag_2GeS_3$ crystal: Experiment and theory. *Spectrochim. Acta A* **2012**, *93*, 274−279.
(53) Aruga, A.; Okamoto, Y. Structure and Photoacoustic Spectra of Ag-doped $Cu_2SiS_3$ particles. *Jpn. J. Appl. Phys.* **2006**, *45*, 4616.
(54) Zhai, Y.-T.; Chen, S.; Yang, J.-H.; Xiang, H.-J.; Gong, X.-G.; Walsh, A.; Kang, J.; Wei, S.-H. Structural diversity and electronic properties of $Cu_2SnX_3$(X=S, Se): A first-principles investigation. *Phys. Rev. B* **2011**, *84*, No. 075213.
(55) Kang, L.; Zhou, M.; Yao, J.; Lin, Z.; Wu, Y.; Chen, C. Metal Thiophosphates with Good Mid-infrared Nonlinear Optical Performances: A First-Principles Prediction and Analysis. *J. Am. Chem. Soc.* **2015**, *137*, 13049−13059.
(56) Lekse, J. W.; Moreau, M. A.; McNerny, K. L.; Yeon, J.; Halasyamani, P. S.; Aitken, J. A. Second-Harmonic Generation and Crystal Structure of the Diamond-like Semiconductors $Li_2CdGeS_4$ and $Li_2CdSnS_4$. *Inorg. Chem.* **2009**, *48*, 7516−7518.
(57) Rosmus, K. A.; Brant, J. A.; Wisneski, S. D.; Clark, D. J.; Kim, Y. S.; Jang, J. I.; Brunetta, C. D.; Zhang, J.-H.; Srnec, M. N.; Aitken, J. A. Optical Nonlinearity in $Cu_2CdSnS_4$ and $\alpha/\beta$-$Cu_2ZnSiS_4$: Diamond-like Semiconductors with High Laser-Damage Thresholds. *Inorg. Chem.* **2014**, *53*, 7809−7811.
(58) Li, D.; Zhu, Z.; Ling, F.; Zhang, X. Theoretical studies of the structural, electronic, and optical properties of Cu2HgGeS4. *Phys. Status Solidi B* **2012**, *249*, 2202−2206.
(59) Gulay, L. D.; Olekseyuk, I. D.; Parasyuk, O. V. Crystal structures of the $Ag_4HgGe_2S_7$ and $Ag_4CdGe_2S_7$ compounds. *J. Alloys Compd.* **2002**, *340*, 157−166.
(60) Yao, W.-D.; Cheng, X.; Guo, S.-P.; Whangbo, M.-H.; Ding, B.; Deng, S. Phase Competition and Strong SHG Responses of the $Li_2M^{II}M^{IV}Se_4$ Family: Atom Response Theory Predictions versus Experimental Results. *Chem. Mater.* **2023**, *35*, 1159−1167.
(61) Sun, M.; Zhang, X.; Xing, W.; Uykur, E.; Yin, W.; Lin, Z.; Yao, J. $Ba_6In_2Ge_2Te_{15}$: a THz birefringent material with an intriguing quasi-$[Te_5]^{4-}$ chain possessing large optical anisotropy and an ultrawide transmission range. *Inorg. Chem. Front.* **2022**, *9*, 3421−3427.
(62) Schunemann, P. G.; Setzler, S. D.; Pollak, T. M.; Ohmer, M. C.; Goldstein, J. T.; Zelmon, D. E. Crystal growth and properties of $AgGaTe_2$. *J. Cryst. Growth* **2000**, *211*, 242−246.
(63) Lin, H.; Chen, H.; Zheng, Y.-J.; Yu, J.-S.; Wu, L.-M. $AX_4^{II}X_5^{III}Te_{12}$ (A = Rb, Cs; $X^{II}$ = Mn, Zn, Cd; $X^{III}$ = Ga, In): quaternary semiconducting tellurides with very low thermal conductivities. *Dalton Trans.* **2016**, *45*, 17606−17609.
(64) Aydın, C.; Abd El-sadek, M.; Zheng, K.; Yahia, I.; Yakuphanoglu, F. Synthesis, diffused reflectance and electrical properties of nanocrystalline Fe-doped ZnO via sol−gel calcination technique. *Opt. Laser Technol.* **2013**, *48*, 447−452.
(65) Sheldrick, G. M. Crystal structure refinement with SHELXL. *Acta Crystallogr. C* **2015**, *71*, 3−8.
(66) Kurtz, S. K.; Perry, T. A powder technique for the evaluation of nonlinear optical materials. *J. Appl. Phys.* **1968**, *39*, 3798−3813.
(67) Clark, S. J.; Segall, M. D.; Pickard, C. J.; Hasnip, P. J.; Probert, M. I.; Refson, K.; Payne, M. C. First principles methods using CASTEP. *Z. Kristallogr. - Cryst. Mater.* **2005**, *220*, 567−570.
(68) Kohn, W.; Sham, L. J. Self-consistent equations including exchange and correlation effects. *Phys. Rev.* **1965**, *140*, A1133.
(69) Hohenberg, P.; Kohn, W. Inhomogeneous electron gas. *Phys. Rev.* **1964**, *136*, B864.
(70) Rappe, A. M.; Rabe, K. M.; Kaxiras, E.; Joannopoulos, J. D. Optimized pseudopotentials. *Phys. Rev. B* **1990**, *41*, 1227−1230.
(71) Lin, J. S.; Qteish, A.; Payne, M. C.; Heine, V. Optimized and transferable nonlocal separable ab initio pseudopotentials. *Phys. Rev. B* **1993**, *47*, 4174−4180.
(72) Lee, M. H.; Lin, J. S.; Payne, M. C.; Heine, V.; Milman, V.; Crampin, S. Kinetic energy tuning for optimising pseudopotentials and projector reduction. *Psi-k Newsl. Highlight* **1994**, 67.
(73) Chen, C.-W.; Lee, M.-H.; Lin, Y.-T. Electro-optical modulation for a boron nitride nanotube probed by first-principles calculations. *Appl. Phys. Lett.* **2006**, *89*, No. 223105.
(74) He, R.; Lin, Z. S.; Lee, M. H.; Chen, C. T. Ab initio studies on the mechanism for linear and nonlinear optical effects in $YAl_3(BO_3)_4$. *J. Appl. Phys.* **2011**, *109*, No. 103510.
(75) Jiang, X.; Kang, L.; Luo, S.; Gong, P.; Lee, M.-H.; Lin, Z. Development of nonlinear optical materials promoted by density functional theory simulations. *Int. J. Mod. Phys. B* **2014**, *28*, No. 1430018.
(76) Lin, H.; Liu, Y.; Zhou, L.-J.; Zhao, H.-J.; Chen, L. Strong Infrared NLO Tellurides with Multifunction: $CsX_4^{II}In_5Te_{12}$ ($X^{II}$ = Mn, Zn, Cd). *Inorg. Chem.* **2016**, *55*, 4470−4475.
(77) Lin, H.; Zhou, L.-J.; Chen, L. Sulfides with Strong Nonlinear Optical Activity and Thermochromism: $ACd_4Ga_5S_{12}$ (A = K, Rb, Cs). *Chem. Mater.* **2012**, *24*, 3406−3414.
(78) Lin, H.; Chen, L.; Zhou, L.-J.; Wu, L.-M. Functionalization Based on the Substitutional Flexibility: Strong Middle IR Nonlinear Optical Selenides $AX_4^{II}X_5^{III}Se_{12}$. *J. Am. Chem. Soc.* **2013**, *135*, 12914−12921.
(79) Zhou, M.; Yang, Y.; Guo, Y.; Lin, Z.; Yao, J.; Wu, Y.; Chen, C. Hg-based infrared nonlinear optical material $KHg_4Ga_5Se_{12}$ exhibits good phase-matchability and exceptional second harmonic generation response. *Chem. Mater.* **2017**, *29*, 7993−8002.
(80) Li, M.-J.; Hu, C.-L.; Lei, X.-W.; Zhou, Y.; Mao, J.-G. Syntheses, crystal and electronic structures of three new potassium cadmium-(II)/zinc(II) tellurides: $K_2Cd_2Te_3$, $K_6CdTe_4$ and $K_2ZnTe_2$. *J. Solid State Chem.* **2009**, *182*, 1245−1251.
(81) Yakuphanoglu, F.; Ilican, S.; Caglar, M.; Caglar, Y. The determination of the optical band and optical constants of non-crystalline and crystalline ZnO thin films deposited by spray pyrolysis. *J. Optoelectron. Adv. Mater.* **2007**, *9*, 2180.
(82) Sun, M.; Li, C.; Shi, J.; Lee, M.-H.; Yao, J. Defect diamond-like tellurides as infrared nonlinear optical materials with giant second-harmonic generation tensor. *Mater. Today Phys.* **2023**, *36*, No. 101166.
(83) Tang, C.; Xing, W.; Liang, F.; Sun, M.; Tang, J.; Lin, Z.; Yao, J.; Chen, K.; Wu, J.; Yin, W.; Kang, B. Structural modification from centrosymmetric $Rb_4Hg_2Ge_2S_8$ to noncentrosymmetric $(Na_3Rb)$-$Hg_2Ge_2S_8$: mixed alkali metals strategy for infrared nonlinear optical material design. *J. Mater. Chem. C* **2022**, *10*, 3300−3306.
(84) Wu, K.; Yang, Z.; Pan, S. $Na_2Hg_3M_2S_8$ (M = Si, Ge, and Sn): New Infrared Nonlinear Optical Materials with Strong Second Harmonic Generation Effects and High Laser-Damage Thresholds. *Chem. Mater.* **2016**, *28*, 2795−2801.
(85) You, S. H.; Hong, K. J.; Jeong, T. S.; Youn, C. J., Point-defect study from low-temperature photoluminescence of $CdGa_2Se_4$ layers through the postannealing in various ambient. *J. Appl. Phys.* 2010, *108* (5), DOI: 10.1063/1.3481347.
(86) Li, Q.; Xue, D.-X.; Zhang, Y.-F.; Zhang, Z.-H.; Gao, Z. Syntheses, crystal structures and photoluminescence properties of five Cd/Zn−organic frameworks. *J. Mol. Struct.* **2018**, *1164*, 123−128.
(87) Hu, J.; Zhao, Y.; Yang, F.; Liao, C.; Zhao, J. Ag/Cd coordination architecture and photoluminescence behaviors. *J. Coord. Chem.* **2018**, *71*, 1368−1379.
(88) Zheng, N.; Bu, X.; Feng, P. Nonaqueous Synthesis and Selective Crystallization of Gallium Sulfide Clusters into Three-Dimensional Photoluminescent Superlattices. *J. Am. Chem. Soc.* **2003**, *125*, 1138−1139.
(89) Machuga, A.; Radu, R.; Pintea, V.; Arama, E.; Zhitar, V.; Shemyakova, T. In *X-Ray* Luminescence in $ZnIn_2S_4$, $CdGa_2S_4$ and $Zn_3In_2S_6$, Semicond. *Conferences* **2007**, *2*, 377−380.
(90) Yu, P.; Zhou, L.-J.; Chen, L. Noncentrosymmetric Inorganic Open-Framework Chalcohalides with Strong Middle IR SHG and Red Emission: $Ba_3AGa_5Se_{10}Cl_2$ (A = Cs, Rb, K). *J. Am. Chem. Soc.* **2012**, *134*, 2227−2235.

(91) Ran, M.-Y.; Ma, Z.; Wu, X.-T.; Lin, H.; Zhu, Q.-L. $Ba_2Ge_2Te_5$: a ternary NLO-active telluride with unusual one-dimensional helical chains and giant second harmonic-generation tensors. *Inorg. Chem. Front.* **2021**, *8*, 4838−4845.
(92) Lin, H.; Chen, H.; Zheng, Y.-J.; Yu, J.-S.; Wu, X.-T.; Wu, L.-M. Coexistence of Strong Second Harmonic Generation Response and Wide Band Gap in $AZn_4Ga_5S_{12}$ (A = K, Rb, Cs) with 3D Diamond-like Frameworks. *Chem. Eur. J.* **2017**, *23*, 10407−10412.



https://doi.org/10.1021/acs.chemmater.3c01493
*Chem. Mater.* 2023, 35, 7218−7228